Journal of Catalysis 285 (2012) 31–40

Contents lists available at SciVerse ScienceDirect

Journal of Catalysis

journal homepage: www.elsevier.com/locate/jcat

Intramolecular selective hydrogenation of cinnamaldehyde over CeO_2–ZrO_2-supported Pt catalysts

S. Bhogeswararao, D. Srinivas *

Catalysis Division, National Chemical Laboratory, Pune 411 008, India

ARTICLE INFO

Article history:
Received 12 May 2011
Revised 12 August 2011
Accepted 6 September 2011
Available online 19 October 2011

Keywords:
Hydrogenation
Cinnamaldehyde
α,β-Unsaturated aldehyde
Ceria–zirconia
Supported Pt catalyst
Promotion by alkali ions

ABSTRACT

Selective liquid phase hydrogenation of cinnamaldehyde is reported, for the first time, over CeO_2, ZrO_2, and CeO_2–ZrO_2-supported Pt catalysts. Cinnamyl alcohol is the selective product. These catalysts are highly active and selective even at 25 °C and found to be superior to most of the hitherto known supported Pt catalysts. Alkali addition (NaOH) has enhanced the performance of these catalysts. At an optimized reaction condition, 95.8% conversion of cinnamaldehyde and 93.4% selectivity of cinnamyl alcohol have been obtained. Acidity of the support (due to the presence of ZrO_2 component) and higher electron density at Pt (due to CeO_2 component) are attributed to be responsible for the superior catalytic activity of Pt supported on CeO_2–ZrO_2 composite material.

1. Introduction

Selective hydrogenation of α,β-unsaturated aldehydes is of both fundamental and industrial importance [1–3]. In such compounds, hydrogenation can occur either at the olefinic (C=C) or carbonyl (C=O) groups (Scheme 1). While the hydrogenation of olefinic group leads to saturated aldehydes, that of carbonyl group yields unsaturated alcohols. Both these hydrogenation products of cinnamaldehyde—a representative α,β-unsaturated aldehyde, are widely used in pharmaceuticals, perfumes, and flavors [4,5]. Recently, hydrocinnamaldehyde was found to be an important intermediate in the preparation of a drug used in the treatment of HIV [6]. Although extensively studied, the selective hydrogenation of α,β-unsaturated aldehydes remains as a challenging task [7–11]. Thermodynamics favor the reduction in C=C group. Selective hydrogenation of the carbonyl group to achieve the corresponding unsaturated alcohol with high yield is quite demanding [1–3]. Stoichiometric reducing agents like metal hydrides, aluminum isopropoxide, etc., can accomplish this selective reduction to unsaturated alcohols [1,4]. But such processes involve costly chemicals and co-produce large amount of waste. Heterogeneous catalysts offer several advantages. A large number of supported Pd, Pt, Rh, Ru, Au, and Co catalysts have been reported for this transformation [7–11]. However, high selectivity at high conversion levels particularly at ambient conditions and catalyst reusability are still issues to be resolved. This is a highly demanding task due to the complexity of the system involving a rather complicated reaction mechanism, including competitive/non-competitive and dissociative/non-dissociative adsorption, side reaction, adsorption of solvent, etc. [2,4,12]. In order to prevent consecutive hydrogenations to the saturated alcohol and the isomerization of the allylic alcohol (Scheme 1), the catalyst has to suppress these reactions. The selectivity to unsaturated alcohol must be controlled by changes in the rate constants of both competitive reactions and in adsorption constants of the components [1]. However, the key factors that control the activity and selectivity in the hydrogenation of cinnamaldehyde are still unclear. Support material and particle size of the metals, selective poisoning, presence of a second metal, preparation method, catalyst precursor, temperature of reduction, pressure, etc., have been proposed to influence the intramolecular hydrogenation selectivity [1].

The selectivity for the unsaturated alcohol can be enhanced by polarization of the C=O group or by hindering the adsorption of the substrate through the C=C group. This can be achieved by a right choice of the support, which can interact with the supported metal [13–15], addition of a more electropositive metal such as iron, tin, or zinc [16–19], or by steric and electronic effects provided by the support [1,19]. Recently, Ramos-Fernández et al. [20] have reported the effect of the support, Al_2O_3 and SiO_2, on the catalytic behavior of Cr–ZnO promoted Pt catalysts. The SiO_2 support enabled high dispersion of the promoter, which, in turn, facilitated high selectivity (>95%) toward the unsaturated alcohols in the hydrogenation of cinnamaldehyde. However, high temperature (110 °C), high pressure

* Corresponding author. Fax: +91 20 2590 2633.
E-mail address: d.srinivas@ncl.res.in (D. Srinivas).

0021-9517/$ - see front matter © 2011 Elsevier Inc. All rights reserved.
doi:10.1016/j.jcat.2011.09.006

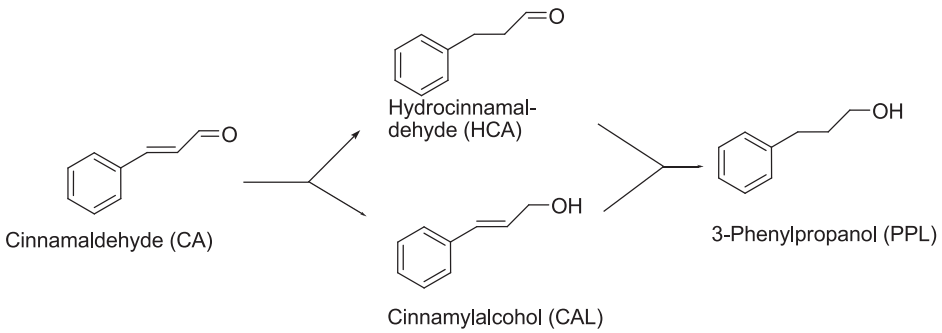

Scheme 1. Hydrogenation products of cinnamaldehyde.

(70 bar), and long reaction times (>10 h) were needed to obtain high conversion of cinnamaldehyde over those catalysts. Teddy et al. [21] studied the influence of alloying in carbon nanotube-supported Pt–Ru catalysts for the selective hydrogenation. High selectivity (94%) toward cinnamyl alcohol together with high activity (cinnamaldehyde conversion = 70%) was obtained through high temperature treatment (1000 °C) of the catalyst. Several years ago, Englisch et al. [22] investigated the effect of polar sites generated on the Pt surface by addition of metals and oxide promoters (Ga, Sn, and Ge) that decorated part of the Pt surface and improved the selectivity toward unsaturated alcohols in the liquid phase hydrogenation of crotonaldehyde. However, this addition of metal and oxide promoters decreased the activity of the catalysts. Coq et al. [23] studied zirconia-supported Ru catalysts and proposed the formation of Ru–ZrO_x sites at the periphery of the Ru particles to explain the enhanced selectivity for cinnamyl alcohol. Although many studies have been conducted on this or other α,β-unsaturated aldehydes using Pt supported on different oxides, a more efficient and selective catalyst that is active even at room temperature and low pressures of H_2 is still not known.

We report here the application of Pt/CeO_2–ZrO_2 catalysts for this reaction. Ceria is a reducible oxide. It facilitates dispersion of Pt and provides good support–metal interactions. Ceria–zirconia solid solutions provide thermal stability and prevent sintering of the supported metals. Presence of zirconia enhances the oxygen storage capacity of ceria. All these superior characteristics of CeO_2–ZrO_2 support are expected to impart higher activity and selectivity in hydrogenation reactions. The ceria-based catalysts are in use in automobile exhaust emission control, fuel cell research, natural gas combustion, total oxidation of hydrocarbons, methanol decomposition, and several other reactions [25–30]. In this study, we have found that the support, electronic structure of the metal, and alkali ion addition influence the conversion and product selectivity. Cinnamyl alcohol (formed via C=O hydrogenation) is the major product. A comparison of these results with those obtained over the Pd catalysts [24] is made. The differences in activity/selectivity are discussed in terms of electronic and redox properties of these catalyst systems.

2. Experimental

2.1. Catalyst preparation

2.1.1. CeO_2–ZrO_2

CeO_2–ZrO_2 composites (Ce/Zr molar ratio = 1:1) were prepared by co-precipitation method [7]. $Ce(NO_3)_3{\cdot}6H_2O$ (7.35 g, Semco) and $ZrO(NO_3)_2{\cdot}xH_2O$ (2.8 g, Loba Chemie) were dissolved separately in distilled water (168 and 120 ml, respectively). These solutions were mixed together and added dropwise to a continuously stirred 0.1 M aq. solution (1 L) of NaOH taken in a 2 L round bottom flask, placed in an oil bath. Stirring was continued for 3 h. During addition, the temperature of the flask was maintained at 80 °C and pH at 10. The cations were precipitated in the form of their hydroxides. The mixture was digested at 80 °C for another 3 h and then cooled to 25 °C. The precipitate was separated and washed with distilled water until all the Na^+ ions were removed. It was, then, air-dried, powdered, and calcined at 450 °C for 2.5 h to get the final product.

Pure ceria and pure zirconia supports were also prepared by the precipitation method.

2.1.2. Pt/CeO_2–ZrO_2

Pt (5 wt%) supported on CeO_2–ZrO_2 was prepared by impregnation method. Tetraaminoplatinum(II) nitrate precursor (1.767 g) $[Pt(NH_3)_4(NO_3)_2$, 3 wt% aqueous solution, Aldrich] taken in 10 ml of distilled water was added to 1 g of CeO_2–ZrO_2 contained in a glass round bottom flask. It was mixed thoroughly and dried at 80 °C using a rotary evaporator. The solid obtained was recovered and dried at 100 °C for 6 h in an electric oven. Then, the material was calcined at 400 °C for 2 h.

Catalyst samples with different Pt loadings (0.5, 1, and 2 wt%) were prepared in a similar manner taking appropriate amounts of platinum precursor.

2.2. Characterization procedures

X-ray diffractograms (XRD) of the catalysts were recorded in the 2θ range of 10–80° (scan rate of 2.3°/min) on a Xpert Pro PANalytical X-ray diffractometer with Ni-filtered Cu Kα radiation (40 kV, 30 mA). The specific surface area (BET) of the samples was determined using a NOVA 1200 Quanta Chrome instrument. The micropore volume was estimated from the *t*-plot, and the pore diameter was determined using the Barret–Joyner–Halenda (BJH) model. Morphological characteristics of the samples were determined using a high resolution transmission electron microscope (HRTEM, JEOL, model 1200 EX) operating at 100 kV. X-ray photoelectron spectra (XPS) of the samples were acquired on a VG Microtech Multilab ESCA 3000 with Mg Kα radiation ($h\nu$ = 1253.6 eV). Base pressure in the analysis chamber was maintained at 3–6×10^{-10} mbar. The peak corresponding to carbon 1s (at 284.2 eV) was taken as a reference in estimating binding energy (BE) values of various elements in the catalyst.

Temperature-programmed desorption of ammonia (NH_3-TPD; Micromeritics Auto Chem 2910 instrument) quantified the density of acid sites. Diffuse-reflectance infrared Fourier transform (DRIFT; Shimadzu SSU 8000) spectroscopy of adsorbed pyridine provided information on the type of acid sites present in the catalyst [24].

Temperature-programmed reduction experiments were carried on a Micromeritics Auto Chem 2920 instrument: 0.05 g of the catalyst was placed in a quartz tube and treated with He gas (20 cc/min) at 200 °C for 1 h. A gas mixture of H_2(5%)–Ar(95%) was then passed (20 cc/min) through the quartz reactor at 40 °C for 1 h.

The temperature was raised to 950 °C at a heating rate of 10°/min and held at 950 °C for 10 min. The amount of hydrogen consumed was estimated, and the reduction capacity of the catalyst was determined. A standard CuO powder was used to calibrate the H_2 consumption.

Fourier transform infrared (FTIR) spectra of adsorbed CO were recorded on a Bruker IFS 88 spectrometer with DTGS detector using OPUS software at a resolution of 4 cm^{-1} over 64 scans. Samples were made in the form of self-supporting wafers (ca. 12 mg/cm^2) of thickness suitable for transmission IR experiments. Samples were directly treated in a specially designed quartz cell equipped with KBr windows, suitable for activation and in situ IR studies. The samples were degassed while increasing the temperature to 450 °C at a slow heating rate (ca. 1–2°C/min), treated with 133 mbar of oxygen at 450 °C for 1 h, and then followed by degassing at that temperature, in order to clean any pre-adsorbed molecules at the active sites. Reduction was carried out under hydrogen (80 mbar) for 1 h after bring down the temperature to 250 °C. Subsequently, the hydrogen was degassed at this temperature and cooled slowly to 25 °C 298 K. Spectra were recorded by gradually increasing the CO equilibrium pressure in the range of 0.001–5 mbar. Spectra were recorded by injecting increasing dosage of known small amounts of CO starting from 0.07 μmol till as high as 50 μmol using a pirani vacuum gauge (Oerlikon Leybold Vakuum Thermovac) after calibrating the glass linings. The catalyst spectrum collected before CO dosage was used as a reference for obtaining the reported background-subtracted spectra. Spectra were normalized with respect to pellet thickness. The particle size of Pt metal was calculated from the dispersion values (CO-FTIR) by considering the surface density of Pt atoms.

2.3. Reaction procedure

Prior to reactions, the catalysts were freshly reduced at 300 °C, for 2 h, in a flow of hydrogen (30 cc/min). Upon reduction, the color of the catalyst changed from dark brown to black. The temperature was brought down to 25 °C. Without exposing to atmosphere, 0.05 g of reduced catalyst was transferred into a Parr reactor (300 ml) containing cinnamaldehyde (4 g; Aldrich Co.) and solvent (40 ml; s.d. fine Chem Ltd., India). The reactor was initially flushed and then pressurized with hydrogen to a desired value (1–30 bar). The reaction was conducted for 2 or 8 h at 25 °C while stirring at a speed of 500 rpm. In kinetic studies, samples were collected at regular intervals of time, diluted with the solvent, and then analyzed and quantified by gas chromatographic technique (Varian 3400; CP-SIL8CB column; 30 m-long and 0.53 mm i.d.). The products were identified by GC–MS (Shimadzu GCMS-QP5050A; HP-5 column; 30 m-long × 0.25 mm i.d. × 0.25 μm thickness). Some experiments were carried out at higher temperatures (50, 75, and 100 °C).

3. Results and discussion

3.1. Structural properties

The ceria–zirconia mixed oxides are formed in different crystalline structures depending on their chemical composition. According to the $Ce_{1-x}Zr_xO_2$ phase diagram, for $x \leqslant 0.15$, a cubic fluorite-type phase is formed and for $x \geqslant 0.85$, a monoclinic phase is obtained [31]. At intermediate compositions, various phases have been identified [31–33]. In other words, the ceria–zirconia material exhibits complex structural characteristics. The mixed oxide composite of the present study showed XRD pattern typical of a mixture of cubic and tetragonal phases with the former being more predominant than the latter (Fig. 1). The peaks due to the tetragonal phase

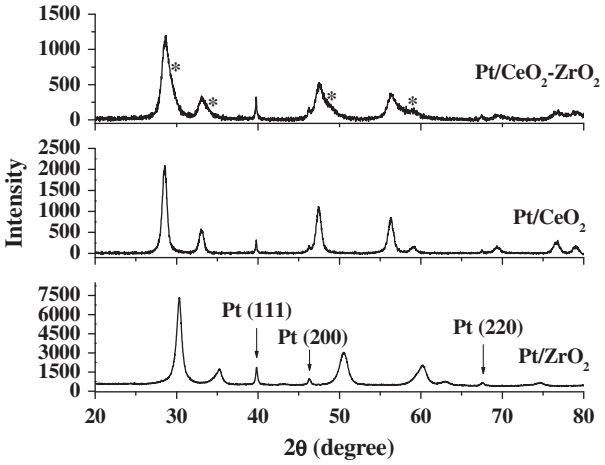

Fig. 1. XRD patterns of the reduced supported Pt (5 wt%) catalysts. Asterisks represent the peaks corresponding to the tetragonal phase of the support. Arrows denote the peaks due to metallic Pt.

(appearing as shoulders) are marked in the figure by asterisks. Recently, Li et al. [34] have also observed a mixed crystallite phase for CeO_2–ZrO_2 prepared at lower temperatures (<500 °C). Neat CeO_2 showed a cubic fluorite structure [35]. The unit cell parameter (a_{cubic}) of "neat" CeO_2–ZrO_2 was smaller (0.537 nm) than "neat" CeO_2 (0.542 nm), suggesting formation of a CeO_2–ZrO_2 solid solution. The ionic radius of Zr^{4+} (0.084 nm) is smaller than that of Ce^{4+} (0.097 nm)/Ce^{3+} (0.112 nm), and hence, a decrease in unit cell parameter of CeO_2–ZrO_2 was observed [36]. The unit cell parameter decreased (from 0.537 to 0.512 nm) also when Pt was impregnated (Table 1). Samples reduced in a flow of hydrogen showed three additional peaks of low intensity at 39.7, 46.1, and 67.7° (Fig. 1) corresponding to reflections from (111), (200), and (220) planes of metallic platinum, respectively. The intensity of (111) reflection for all these supported Pt samples of the present study is higher than that of the other two, indicating that these planes are preferentially oriented to the others. Jung et al. [37] found a preferential orientation of (111) plane when Pt was supported on herringbone carbon nanofibers and of (220) plane when it was supported on alumina. Support and the method of preparation can influence the orientation of metal crystallites. Using Debye–Scherrer formula and the XRD peak corresponding to (111) reflection, the crystallite size of X-ray detectable metallic Pt on CeO_2, CeO_2–ZrO_2, and ZrO_2 was estimated to be 57.2, 50.5, and 34.2 nm, respectively.

Representative HRTEM images of Pt supported on CeO_2 and CeO_2–ZrO_2 are shown in Fig. 2. From these micrographs, the particle size of Pt was found to be in the range of 5–12 nm. There are a few particles that are of 40 nm size. The values of Pt crystallite sizes determined from XRD measurements are higher than those evaluated from HRTEM. The Pt peak profile in XRD can be separated into two contributions: that corresponding to large crystallites in the thin part of the Pt peaks and to small crystallites in the tails of the diffraction line. The values reported from XRD are those for the large crystallites. From the lattice fringes, we have found that the (111) plane of Pt is preferentially exposed, which agrees well with the inference derived from the XRD results.

3.2. Temperature-programmed reduction and CO adsorption

While XRD and HRTEM, respectively, enabled information on crystallite and particle sizes of supported metallic Pt, temperature-programmed reduction with hydrogen (H_2-TPR) and in situ DRIFTS measurements of adsorbed CO provided knowledge on

Table 1
Physicochemical properties of CeO_2–ZrO_2-supported Pt catalysts.

Sample	XRD			N_2 adsorption–desorption			Acidity (NH_3-TPD, mmol/g)	H_2 uptake – Pt (TPR, mmol/g)
	Support		Average crystallite size of Pt (nm)	S_{BET} (m^2/g)	Pore volume (cm^3/g)	Average pore diameter (nm)		
	Lattice parameter (a_{cubic}, nm)	Average crystallite size (nm)						
CeO_2–ZrO_2	0.537	7.72 (cubic) 7.314 (tetra)	–	115	0.17	6.1	0.179	–
Pt (5 wt%)/CeO_2	0.512	14.07	57.2	91	0.16	6.9	0.295	0.270
Pt (5 wt%)/ZrO_2	0.509	11.9	34.2	107	0.16	6.0	0.440	0.236
Pt (5 wt%)/CeO_2–ZrO_2	0.512	10.97 (cubic), 6.5 (tetragonal)	50.5	94	0.14	5.9	0.367	0.376

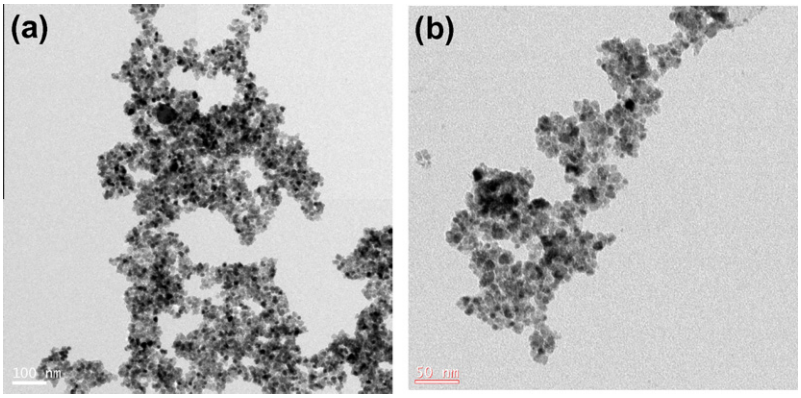

Fig. 2. HRTEM images of: (a) Pt(5 wt%)/CeO_2 and (b) Pt(5 wt%)/CeO_2–ZrO_2 reduced samples.

metal dispersion and support–metal interactions. Bulk platinum shows a hydrogen uptake peak in TPR at 130–160 °C. This peak for Pt supported on CeO_2 (70 and 106 °C) and CeO_2–ZrO_2 (80 and 149 °C) occurred at lower temperatures possibly due to support–metal interactions and variation in crystallite/particle sizes (Fig. 3). CeO_2 is a reducible oxide and keeps the metal in lower oxidation state. While the peak at 80 °C in Pt/CeO_2–ZrO_2 is attributed to Pt strongly interacting with the support, that at 149 °C is attributed to relatively larger size Pt crystallites. These hydrogen uptake peaks in the case of Pt supported on ZrO_2 were observed at 98° and 184 °C, respectively. Neat CeO_2 showed a broad reduction peak centered at 850 °C. In CeO_2–ZrO_2, this peak due to CeO_2 reduction had shifted to lower temperatures (376 and 494 °C) due formation of a CeO_2–ZrO_2 solid solution. These experiments, thus, provide definite evidence that the reduction peaks observed below 184 °C in the case of supported Pt catalysts are due to metal only and not because of the support oxide. The amount of hydrogen uptake by these catalysts was found to decrease in the order: Pt/CeO_2–ZrO_2 (0.376 mmol/g) > Pt/CeO_2 (0.270 mmol/g) > Pt/ZrO_2 (0.236 mmol/g) (Table 1). This observation indicates that the extent of dispersion and the amount of exposed Pt are higher on CeO_2–ZrO_2 than on the other supports.

Metal dispersion was estimated also from the DRIFT spectra of the adsorbed CO of the catalyst samples. Representative CO adsorption profiles for Pt/CeO_2–ZrO_2 at different CO dosages are shown in Fig. 4. It was assumed that one mole of surface Pt adsorbs one mole of CO. It was also presumed that the surface Pt was very sensitive to gas molecules at ambient temperatures and the adsorption is irreversible. On the basis of these assumptions, Pt will adsorb CO irrespective of the CO partial pressure, i.e. as long as free surface Pt sites are available, it will keep on adsorbing CO until all CO present is consumed. Based on this, small doses of calculated amount of CO were injected into the vacuum line and the spectra were recorded. Unless all the surface of Pt is consumed upon each injection, the resultant partial pressure in the line shows zero reading. Once each surface Pt atom is consumed in Pt—CO bond formation, further injection of CO leads to no further increase in CO adsorption as indicated by no (or negligible) drop of pressure and thus no significant increase in integrated intensity of the absorption band (bands). Thus, a plot of integrated intensity verses CO dosage (Fig. 4, right panel) shows a straight line passing through origin (i.e. until no surface Pt is left unsatisfied) and then an almost horizontal line to *X*-axis. The intersection of these two lines gives the point i.e. amount of CO required for consumption

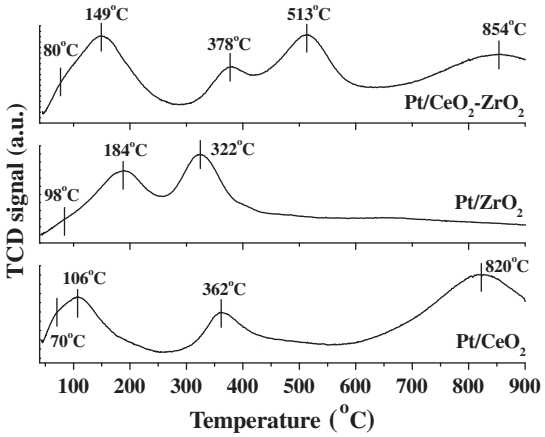

Fig. 3. Temperature-programmed reduction (H_2) profiles of Pt (5 wt%) supported on ZrO_2, CeO_2 and CeO_2–ZrO_2.

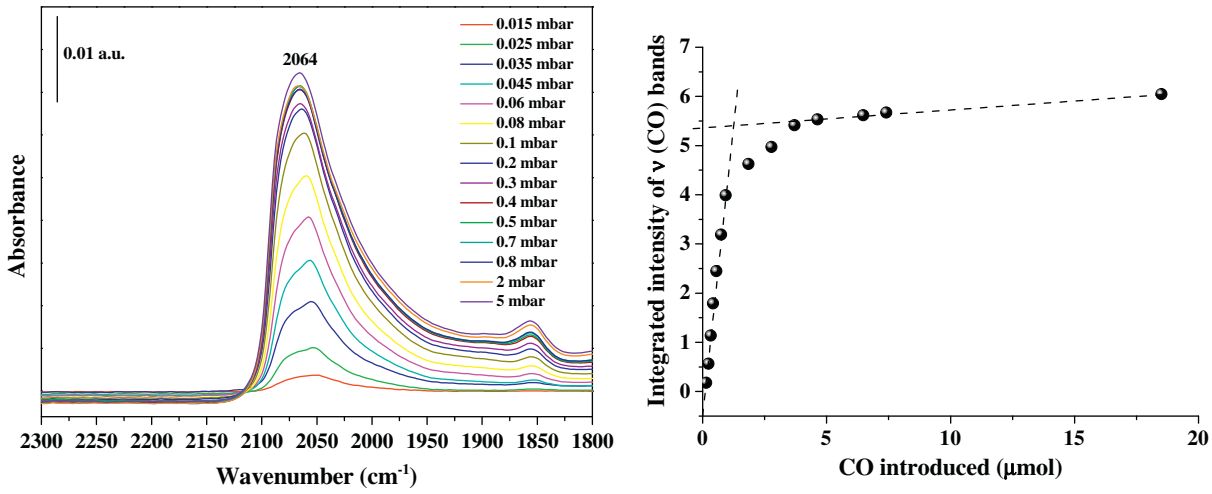

Fig. 4. FTIR spectra of CO adsorbed on Pt (5 wt%)/CeO_2–ZrO_2 catalyst.

Table 2
Binding energy values (in eVs) of supported Pt catalysts.

Sample	Pt^0		Pt^{2+}	
	$4f_{7/2}$	$4f_{5/2}$	$4f_{7/2}$	$4f_{5/2}$
Pt (5 wt%)/CeO_2	70.7	74.1	72.4	75.5
Pt (5 wt%)ZrO_2	70.9	74.6	72.2	75.7
Pt (5 wt%)/CeO_2–ZrO_2	71.3	74.6	72.5	75.8

by surface Pt atoms. Thus, by counting the amount of CO, the amount of surface Pt atoms was calculated.

Two overlapping IR bands at 2058 and 2078 cm^{-1} were observed (Fig. 4). On the basis of earlier reports [38,39], the former is attributed to CO linearly bonded to low-coordinated, open Pt atoms, and the latter to Pt adsorbed at terrace sites. The position of the former shifted to 2064 cm^{-1} as the dosing of CO was increased. Also, a weak band was observed at 1854 cm^{-1} attributable to bridge bonded CO. Observation of this peak indicates that there are also a few number of small size metallic Pt particle on the surface of CeO_2–ZrO_2. In other words, the CO adsorption studies, in concurrence with HRTEM, reveal the presence of different types of Pt particles whose concentration determines the hydrogenation selectivity. On the basis of these CO adsorption studies, metal dispersion on different supports was estimated to increase in the order: Pt(5%)/ZrO_2 (16.2%) < Pt(5%)/CeO_2 (20.3%) < Pt(5%)/CeO_2–ZrO_2 (40.5%). Incorporation of ZrO_2 in CeO_2 promoted the dispersion of Pt by nearly two times. This is a quite high dispersion value, indicating that approximately the half of platinum atoms is located at the surface. However, the crystallite size, as measured from Scherrer equation (XRD), indicated quite large crystal size (50.5 nm). These large crystal sizes strongly indicate that the dispersion of platinum is low, much lower than 40.5%. HRTEM (Fig. 2), on the other hand, showed the presence of a large number of platinum particles of dimension 5–12 nm along with some particles of much larger size. Croy et al. [40] and Dömök et al. [41] demonstrated that the binding energy (BE) values of photoelectrons ejected from metal particles depend on the metal particle size. The smaller the species, the higher would be the binding energy. The BE values of Pt supported on CeO_2–ZrO_2 are higher than those of CeO_2 and ZrO_2 (Table 2). This experimental observation also points out the presence of a large number of smaller size Pt particles on CeO_2–ZrO_2 support. The observed metal dispersion from CO adsorption studies (40.5% for Pt (5%)/CeO_2–ZrO_2) is due to a stoichiometric average of crystals of smaller as well as larger dimensions.

3.3. X-ray photoelectron spectroscopy

The electronic structure of Pt was determined using X-ray photoelectron spectroscopy. Fig. 5 shows the binding energy (B.E.) peaks arising from the 4f core levels of reduced Pt (5 wt%) supported on CeO_2, ZrO_2 and CeO_2–ZrO_2. The peaks at 70.7 and 74.1 eV for Pt/CeO_2 are corresponded to $4f_{7/2}$ and $4f_{5/2}$ levels of Pt^0. The positions of these peaks are in agreement with the values

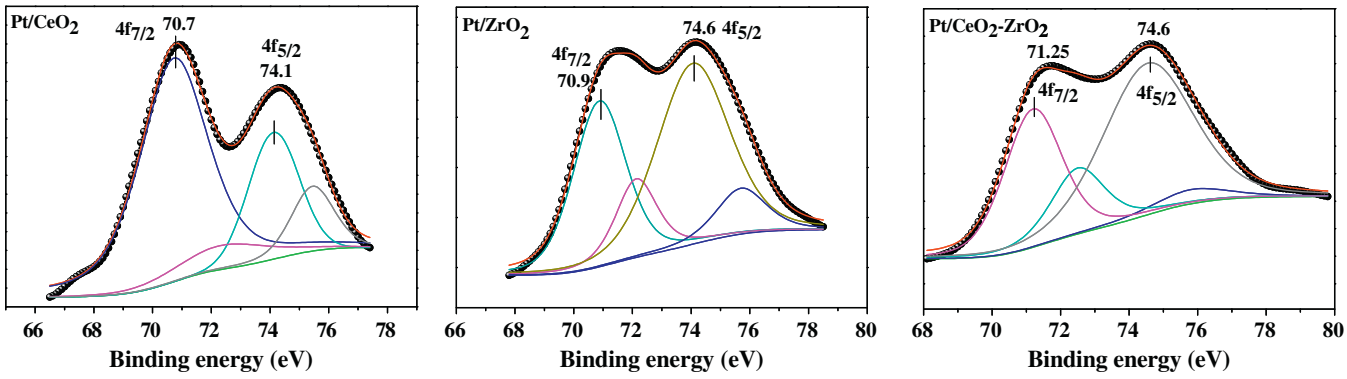

Fig. 5. XPS of 5 wt% Pt supported on CeO_2, ZrO_2, and CeO_2–ZrO_2. Prior to experiments, the catalysts were reduced at 300 °C for 2 h. $4f_{7/2}$ and $4f_{5/2}$ peaks of Pt^0 are indexed. The additional two unresolved peaks in small intensity are due to PtO.

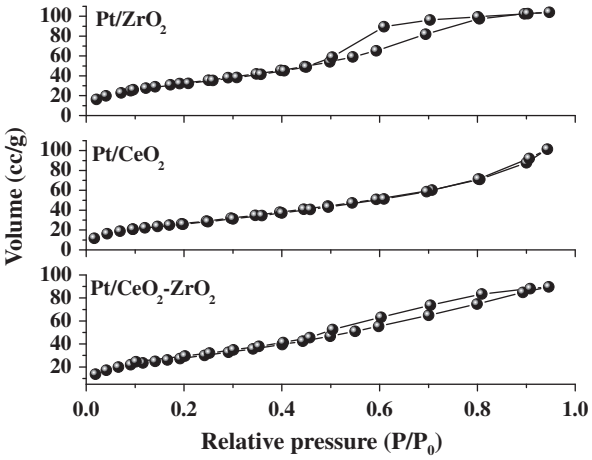

Fig. 6. N_2 adsorption–desorption isotherms of 5 wt% Pt supported on ZrO_2, CeO_2, and CeO_2–ZrO_2 (prior to experiments, catalyst samples were reduced at 300 °C for 2 h).

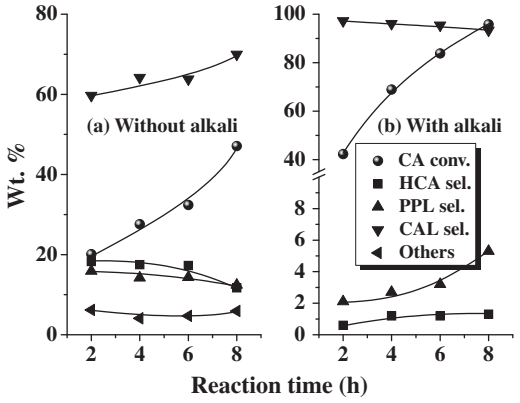

Fig. 8. Influence of alkali addition on the hydrogenation of cinnamaldehyde over Pt (5 wt%)/CeO_2–ZrO_2. *Reaction conditions*: Catalyst (reduced at 300 °C for 2 h) = 0.05 g, cinnamaldehyde (CA) = 4 g, solvent (iso-propanol) = 40 ml, alkali solution = 0.02 g of NaOH in 10 ml water (pH = 13), H_2 pressure = 20 bar, reaction temperature = 25 °C, stirring speed = 500 rpm. HCA = hydrocinnamaldehyde, PPL = 3-phenylpropanol, CAL = cinnamyl alcohol, other products include acetals.

reported by others [42]. Deconvolution of the peaks revealed the presence of oxidized form of platinum (Pt^{2+}) with peaks at 72.4 and 75.5 eV, the concentration of which is small (Table 2). Pt (5 wt%)/ZrO_2 showed the peaks due to Pt^0 at 70.9 and 74.6 eV. These for Pt (5 wt%)/CeO_2–ZrO_2 occurred at 71.3 and 74.6 eV. On the basis of these peak positions, it can be concluded that Pt on CeO_2 is relatively rich in electron density than that supported on ZrO_2 and CeO_2–ZrO_2. It is also likely that the crystallites of Pt are smaller on CeO_2–ZrO_2 than on neat ZrO_2 and CeO_2 [40,41].

3.4. Textural properties

All these materials showed typical type IV isotherms with H3 hysterisis loops (Fig. 6). The specific surface area (S_{BET}) of different catalysts decreased in the order: Pt/ZrO_2 (107 m^2/g) > Pt/CeO_2–ZrO_2 (94 m^2/g) > Pt/CeO_2 (91 m^2/g) (Table 1). Upon Pt impregnation, S_{BET} of CeO_2–ZrO_2 had decreased from 115 to 107 m^2/g.

3.5. Acidic properties: NH_3-TPD and DRIFT spectroscopy of adsorbed pyridine

The density of acid sites on supported Pt catalysts was quantified by NH_3-TPD measurements (Fig. 7 (left panel) and Table 1). Two overlapping, broad desorption peaks were observed in the temperature range 100–400 °C. While the peak at 150–175 °C is attributed to NH_3 desorbed from the surface hydroxyl groups, that at 250–275 °C is corresponded to weak Lewis acid sites [13]. Metal impregnation enhanced the acidity (Table 1). The acidity (NH_3 desorption) of the supported Pt catalysts increased in the order: Pt/CeO_2 (0.295 mmol/g) < Pt/CeO_2–ZrO_2 (0.367 mmol/g) < Pt/ZrO_2 (0.440 mmol/g).

The nature and type of acid sites on CeO_2–ZrO_2 were determined by DRIFT spectroscopy using pyridine as probe molecule (Fig. 7 (right panel)). The sample showed IR peaks of adsorbed pyridine at 1608, 1597, 1485, and 1440 cm^{-1} (Fig. 7 (right panel)). The peaks at 1608 and 1440 cm^{-1} are attributed to H-bonded pyridine, and those at 1597 and 1485 cm^{-1} are assigned to pyridine coordinated to weak Lewis acid sites [43]. Strong Lewis (IR peaks at 1623 and 1455 cm^{-1}) and Brönsted acid sites (1639 and 1546 cm^{-1}) were absent. Upon impregnation of Pt, the relative concentration of these acidic sites has changed (note the change in the intensity of peak at 1485 cm^{-1} in Fig. 7 (right panel)).

3.6. Catalytic activity

Supported Pt catalysts of the present study are highly efficient even at room temperature (25 °C) for the hydrogenation of cinnamaldehyde (CA). Fig. 8 shows the variation of CA conversion and

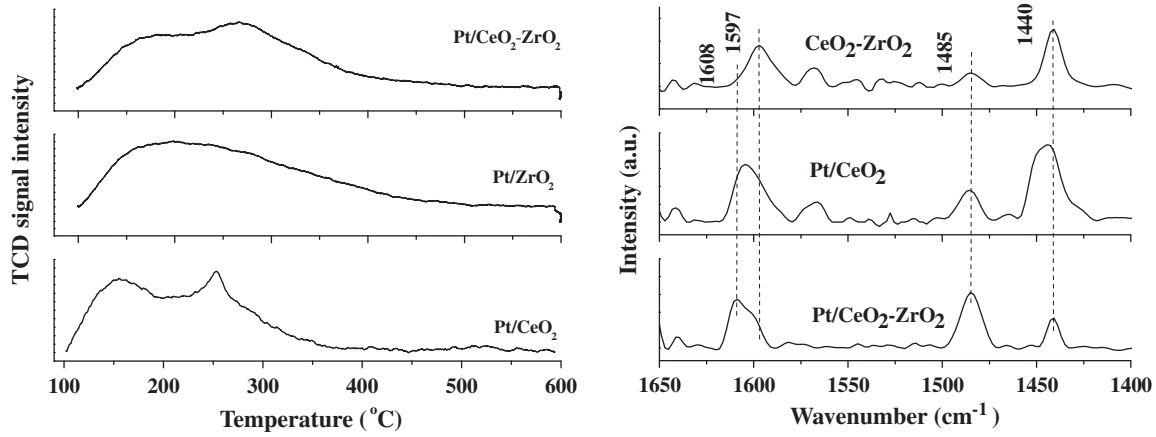

Fig. 7. Left: NH_3-TPD profiles of 5 wt% Pt loaded on CeO_2–ZrO_2, ZrO_2 and CeO_2 (prior to experiment, catalyst samples were reduced at 300 °C for 2 h). Right: DRIFT spectra of adsorbed pyridine.

Table 3
Influence of base on hydrogenation of cinnamaldehyde over Pt (5 wt%)/CeO_2–ZrO_2.

Base	CA conversion (wt%)	TOF (h^{-1})	Product selectivity (%)		
			HCA	PPL	CAL
NaOH	42.3	1233	0.6	2.1	97.3
Na_2CO_3	36.3	1058	26.4	12.0	61.6
$NaHCO_3$	36.5	1064	18.8	8.9	72.3
$(COONa)_2$	40. 6	1184	14.6	8.9	76.5
Na_2SO_4	39.7	1158	16.0	9.7	74.3
KOH	36.0	1050	17.2	8.8	74.0
$Cs(OH)_2$	27.9	813	16.2	11.0	72.8

Reaction conditions: Catalyst (Pt (5 wt%)/CeO_2–ZrO_2 reduced at 300 °C for 2 h) = 0.05 g, cinnamaldehyde (CA) = 4 g, solvent (iso-propanol) = 40 ml, base = 0.02 g (in 10 ml water), H_2 pressure = 20 bar, reaction temperature = 25 °C, reaction time = 2 h, stirring speed = 500 rpm. Turnover frequency (TOF) = moles of CA converted per mole of exposed Pt (derived from CO adsorption studies) per hour. HCA = hydrocinnamaldehyde, PPL = 3-phenylpropanol, CAL = cinnamyl alcohol. No other products (acetals) formed in these reactions.

product selectivity as a function of reaction time for Pt (5 wt%)/CeO_2–ZrO_2 catalyst. This reaction usually yields different hydrogenated products as shown in Scheme 1. Hydrogenation of the carbonyl group (1,2-addition) results in unsaturated alcohol–cinnamyl alcohol (CAL), and hydrogenation of the olefinic bond (3,4-addition) provides the saturated aldehyde–hydrocinnamaldehyde (HCA). The 1,4-addition gives enol, which isomerizes into HCA. Further hydrogenation leads to the formation of 3-phenylpropanol (PPL) and subsequently, propylbenzene (PB). Also, CAL can get reduced to PPL. In the present study, over supported Pt catalysts, 1,2-addition is more selective than 3,4 and 1,4-additions. This is in contrast to that observed over supported Pd catalysts [24] where 3,4, and 1,4-addition products were predominant at all conversion levels. Over Pt(5 wt%)/CeO_2–ZrO_2, CAL formed with a selectivity of 60–70%, while HCA + PPL together formed with a selectivity of 23–33% (Fig. 8). Formation of a minor quantity of acetal side product (selectivity = 4–6%) was also detected. At the end of 8 h, CA conversion was 47.1%. Formation of PB was not detected.

3.6.1. Effect of alkali addition

When alkali (0.02 g of NaOH in 10 ml of water) was added to the reaction medium, a significant enhancement in catalytic activity was observed (Fig. 8). At 8 h, CA conversion increased from 47.1% to 95.8%, turnover frequency (TOF; moles of CA converted per mole of exposed Pt per hour) increased from 343 to 698, and CAL selectivity increased from 70% to 93.4%. Side reactions (acetal formation) got completely suppressed. Several bases including NaOH, KOH, $Cs(OH)_2$, $NaHCO_3$, Na_2CO_3, $(COONa)_2$, and Na_2SO_4 were examined. Among all these, NaOH was found to provide high catalytic activity and CAL selectivity (Table 3).

3.6.2. Effect of solvent

Further, the nature of solvent was found to have a profound influence on CA conversion and CAL selectivity (Table 4). The reactions were conducted in non-polar (toluene) and polar–aprotic (dioxane and acetonitrile) and protic (ethanol, iso-propanol, and tert-butanol) solvents. CA conversion is much higher in ethanol and iso-propanol than in other solvents (TOF = 843 and 586, respectively). However, formation of undesired acetal products was detected in the presence of alcohol solvents. Extent of this is lower in iso-propanol than in ethanol (Table 4). As noted from Table 3, when base (NaOH) was added to the reaction mixture, the side reactions were suppressed and CAL formed selectively. In toluene and acetonitrile solvents, hydrogenation of olefinic bond was preferred to the carbonyl bond of CA. In view of higher apparent activity and CAL selectivity, iso-propanol was chosen as the solvent of choice in further studies.

3.6.3. Effect of Pt loading

Metal loading is essential to get high yields of CAL. As seen from Table 5, CA conversion increased with increasing amount of Pt loading. Conversion of CA increased from 70.4% to 95.8% when the Pt loading on CeO_2–ZrO_2 support was increased from 0.5 to 5 wt%. Only a marginal variation in CAL selectivity (89–93.4%) was observed. This suggests a uniform dispersion of Pt on CeO_2–ZrO_2 support up to a metal loading of at least 5 wt%.

3.6.4. Effect of reaction temperature

The effect of reaction temperature was studied in the absence of alkali promoters as the conversions were lower without alkali addition and the effect of temperature on the reaction can be monitored better. The reactions were conducted at 25, 50, 75, and 100 °C. As seen from Table 6, CA conversion increased from 20.1% to 63.4% for 2 h as the temperature was raised from 25 to 100 °C. Increase in CAL selectivity from 60% to 71% at the expense of HCA + PPL product selectivity was also noted. This study thus reveals that although Pt is effective even at 25 °C for the selective hydrogenation of carbonyl group of CA, temperature further facilitates this selective transformation.

3.6.5. Effect of hydrogen pressure

Hydrogen pressure was varied from 1 to 30 bar while keeping the other parameters unchanged. CA conversion and CAL selectivity have increased with increasing hydrogen pressure (Table 7). A pressure of 20 bar was found optimum to yield CA conversion of 95.8% and CAL selectivity of 93.4% at end of 8 h at 25 °C.

3.6.6. Effect of catalyst amount

CA conversion increased (Table 8) with increasing amount of catalyst from 0.025 to 0.15 g. However, the selectivity for CAL had decreased. At higher amounts of the catalyst, acidity of the

Table 4
Influence of solvent on hydrogenation of cinnamaldehyde over Pt (5 wt%)/CeO_2–ZrO_2.

Solvent	Solvent properties				CA conversion (wt%)	TOF (h^{-1})	Product selectivity (%)			
	Polarity index	Dielectric constant (Debye)	Miscibility in water (%)	Gutmann acceptor number			HCA	PPL	CAL	Others
Isopropanol	3.9	17.9	100	33.8	20.1	586	18.3	15.9	59.7	6.2
Acetonitrile	5.8	36.6	100	18.9	4.9	143	42.6	11.8	45.5	0
Toluene	2.4	2.38	0.051		3.0	87	47.1	27.2	25.7	0
Dioxane	4.8	2.25	100	10.3	10.6	309	24.1	12.5	63.4	0
Ethanol	5.2	24.3	100	37.9	28.9	843	9.9	8.1	47.3	34.7
Tert-butanol	4.0	18	0.43	36.8	10.0	292	19.9	10.9	69.1	0

Reaction conditions: Catalyst (Pt (5 wt%)/CeO_2–ZrO_2 reduced at 300 °C for 2 h) = 0.05 g, cinnamaldehyde (CA) = 4 g, solvent = 40 ml, promoter alkali = nil, H_2 pressure = 20 bar, reaction temperature = 25 °C, reaction time = 2 h, stirring speed = 500 rpm. Turnover frequency (TOF) = moles of CA converted per mole of exposed Pt (derived from CO adsorption studies) per hour. HCA = hydrocinnamaldehyde, PPL = 3-phenylpropanol, CAL = cinnamyl alcohol, other products include acetals.

Table 5
Influence of percentage metal loading on hydrogenation of cinnamaldehyde.

Pt loading (wt%)	CA conversion (wt%)	Product selectivity (%)			
		HCA	PPL	CAL	Others
0.5	70.4	1.9	2.0	89.1	7.0
1	78.2	3.4	2.8	82.5	11.3
2	85.0	1.1	2.5	90.5	5.9
5	95.8	1.3	5.3	93.4	0

Reaction conditions: Catalyst (Pt/CeO_2–ZrO_2 reduced at 300 °C for 2 h) = 0.05 g, cinnamaldehyde (CA) = 4 g, solvent (iso-propanol) = 40 ml, alkali solution = 0.02 g of NaOH in 10 ml water (pH = 13), H_2 pressure = 20 bar, reaction temperature = 25 °C, reaction time = 8 h, stirring speed = 500 rpm. HCA = hydrocinnamaldehyde, PPL = 3-phenylpropanol, CAL = cinnamyl alcohol, other products include acetals.

medium increases, which facilitates activation of olefinic bonds and formation of acetal products. An amount of 0.05 g of catalyst was found ideal at our reaction conditions. The selectivity to CAL verses conversion plots, as varied by changing the amount of catalyst in the reactor (Table 8) and by changing the reaction time (Fig. 8), showed a similar trend. The selectivity to CAL decreased with increasing conversion. At the same time, some increase in the selectivity to PPL (formed via further hydrogenation of CAL) was noted. This variation in product selectivity with conversion follows the trend proposed in the reaction Scheme 1.

3.6.7. Effect of support

Fig. 9 demonstrates the influence of support on the catalytic activity and product selectivity of the Pt catalysts. CeO_2–ZrO_2 was found to be a better support than neat CeO_2 and neat ZrO_2. While CA conversion was 95.8% with CAL selectivity of 93.4% at the end of 8 h, by using Pt (5%)/CeO_2–ZrO_2, the conversion was only 88.9 and 81.8% on Pt (5 wt%)/CeO_2 and Pt (5 wt%)/ZrO_2, respectively. In the presence of zirconia, the activity and selectivity (for CAL) of ceria has increased.

Table 9 compares the catalytic activity of Pt/CeO_2–ZrO_2 with that of other reported catalysts. High amount of catalyst and temperature are the requirements with most of the known catalysts. They are either poorly active or less selective. The catalyst of the present study shows efficient activity and selectivity even at ambient temperature (25 °C).

3.7. Structure–activity correlation

The catalysts of the present work are highly active and selective for the hydrogenation of CA even at 25 °C and H_2 pressures as low

Table 6
Effect of reaction temperature on the hydrogenation of cinnamaldehyde over Pt (5 wt%)/CeO_2–ZrO_2.

Temperature (°C)	CA conversion (wt%)	TOF (h^{-1})	Product selectivity (%)			
			HCA	PPL	CAL	Other products
25	20.1	586	18.3	15.9	59.7	6.2
50	39.3	1146	14.3	12.7	64.9	8.1
75	43.5	1268	15.3	11.3	66.9	6.5
100	63.4	1849	10.8	13.1	71.1	5.0

Reaction conditions: Catalyst (reduced at 300 °C for 2 h) = 0.05 g, cinnamaldehyde (CA) = 4 g, solvent (iso-propanol) = 40 ml, alkali addition = nil, H_2 pressure = 20 bar, reaction time = 2 h, stirring speed = 500 rpm. Turnover frequency (TOF) = moles of CA converted per mole of exposed Pt (derived from CO adsorption studies) per hour. HCA = hydrocinnamaldehyde, PPL = 3-phenylpropanol, CAL = cinnamyl alcohol, other products include acetals.

Table 7
Effect of H_2 pressure:hydrogenation of cinnamaldehyde over Pt (5 wt%)/CeO_2–ZrO_2.

H_2 pressure (bar)	CA conversion (wt%)	TOF (h^{-1})	Product selectivity (%)			
			HCA	PPL	CAL	Others
1	17.0	124	28.5	4.8	66.8	0
5	40.0	292	11.6	6.4	82.0	0
10	80.7	588	3.2	3.2	89.6	4.1
20	95.8	698	1.3	5.3	93.4	0
30	99.2	723	0.1	10.2	89.6	0

Reaction conditions: Catalyst (Pt/CeO_2–ZrO_2 reduced at 300 °C for 2 h) = 0.05 g, cinnamaldehyde (CA) = 4 g, solvent (iso-propanol) = 40 ml, alkali solution = 0.02 g of NaOH in 10 ml water (pH = 13), reaction temperature = 25 °C, reaction time = 8 h, stirring speed = 500 rpm. Turnover frequency (TOF) = moles of CA converted per mole of exposed Pt (derived from CO adsorption studies) per hour. HCA = hydrocinnamaldehyde, PPL = 3-phenylpropanol, CAL = cinnamyl alcohol, other products include acetals.

Table 8
Influence of amount of catalyst on hydrogenation of cinnamaldehyde over Pt (5 wt%)/CeO_2–ZrO_2.

Catalyst amount (g)	CA conversion (wt%)	TOF (h^{-1})	Product selectivity (%)			
			HCA	PPL	CAL	Others
0.025	33.7	491	11.8	5.9	82.3	0
0.050	40.0	292	11.7	6.4	82.0	0
0.075	42.2	205	17.8	7.7	74.5	0
0.1	75.0	273	10.6	6.1	75.9	7.5
0.15	86.4	210	20.5	9.3	68.8	1.4

Reaction conditions: Catalyst = Pt (5 wt%)/CeO_2–ZrO_2 reduced at 300 °C for 2 h, cinnamaldehyde (CA) = 4 g, solvent (iso-propanol) = 40 ml, alkali solution = 0.02 g of NaOH in 10 ml water (pH = 13), H_2 pressure = 5 bar, reaction temperature = 25 °C, reaction time = 8 h, stirring speed = 500 rpm. Turnover frequency (TOF) = moles of CA converted per mole of exposed Pt (derived from CO adsorption studies) per hour. HCA = hydrocinnamaldehyde, PPL = 3-phenylpropanol, CAL = cinnamyl alcohol, other products include acetals.

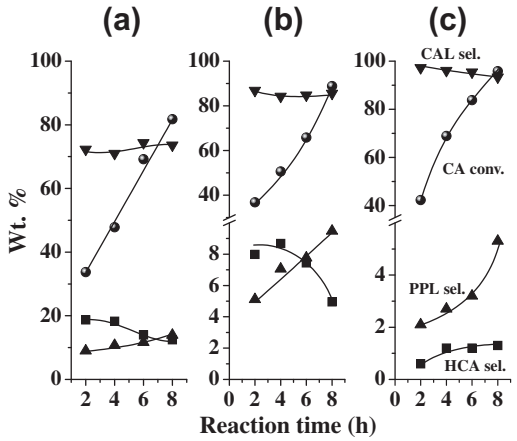

Fig. 9. Influence of support on hydrogenation of cinnamaldehyde: (a) Pt(5 wt%)/ZrO_2, (b) Pt (5 wt%)/CeO_2, and (c) Pt(5 wt%)/CeO_2–ZrO_2. *Reaction conditions*: Catalyst reduced at 300 °C for 2 h = 0.05 g, cinnamaldehyde (CA) = 4 g, solvent (iso-propanol) = 40 ml, alkali solution = 0.02 g of NaOH in 10 ml water (pH = 13), H_2 pressure = 20 bar, reaction temperature = 25 °C, stirring speed = 500 rpm. HCA = hydrocinnamaldehyde, PPL = 3-phenylpropanol, CAL = cinnamyl alcohol, other products include acetals.

as 20 bar. Cinnamyl alcohol is the major product. CA conversion at the end of 8 h over these catalysts increased in the order: Pt/ZrO_2 (81.8%) < Pt/CeO_2 (88.9%) < Pt/CeO_2–ZrO_2 (95.8%), and the selectivity for CAL increased in the order: Pt/ZrO_2 (73.6%) < Pt/CeO_2 (85.6%) < Pt/CeO_2–ZrO_2 (93.4%). The selectivity in the hydrogenation of cinnamaldehyde is affected by the metal particle size. An increase in metal particle size (>3 nm) favors selectivity toward the unsaturated alcohols (CAL). Gallezot and Richard [1] have explained this on the basis of steric effects, wherein with large metal particles, the aromatic ring restrains a close approach of the C=C bond to the metal surface. But on small metal particles, the aromatic ring can lie aside of the metal particle and the C=C bond can be hydrogenated. Originally, Loffreda et al. [52,53] and Serrano-Ruiz et al. [54] explained based on theoretical calculations that the α,β-unsaturated aldehydes adsorb in a different way on different crystal planes and steps. While on Pt(1 1 1) plane, CA prefers to adsorb through η^1(C=O) coordination; on Pt(1 0 0), the adsorption is through both η^2(C=C) and η^1(C=O) modes. With increasing crystallite size, the fraction of steps and corners decreases and (1 1 1) planes are preferentially oriented. The particle size of Pt in the catalysts of present work is 5–12 nm. A few particles of 40 nm were also observed (HRTEM). Hence, as expected (1 1 1), plane is more exposed (XRD and HRTEM), and thereby, the catalysts of this study are more selective for the CAL product.

As seen from CO adsorption studies, support influenced to a great extent the Pt dispersion. Dispersion of Pt is more on CeO_2–ZrO_2 (40.5%) than on CeO_2 (20.3%) and ZrO_2 (16.2%). It is interesting to note that variation in catalytic activity (CA conversion; Fig. 9) is in line with the variation in metal dispersion.

The acidity of different catalysts increased in the order: Pt/CeO_2 (0.295 mmol/g) < Pt/CeO_2–ZrO_2 (0.367 mmol/g) < Pt/ZrO_2 (0.440 mmol/g). This led to unwanted side reactions (acetal formation). Lewis acidity facilitated adsorption of CA through its carbonyl group and enabled selective formation of CAL product. As seen from the XPS data (Table 2), CeO_2 (a reducible metal oxide) promoted electron density at the site of Pt. Higher electron density on metal facilitates π^*_{CO} back bonding, and thereby, an enhancement in the selectivity to CAL during the hydrogenation of CA is observed. The factors of acidity of the support (due to the presence of ZrO_2 component) and higher electron density at Pt (due to CeO_2 component) are responsible for the higher catalytic activity and selectivity of Pt supported on CeO_2–ZrO_2 composite material.

Addition of base to the reaction medium suppressed the side reactions. Apart from altering the electronic structure of metal [24], the alkali ions (Na^+) have also facilitated the adsorption of CA through their carbonyl groups and thereby enhanced the catalytic activity and CAL selectivity.

The physical properties of solvents used in the present study are listed in Table 4 along with the catalytic activity data. Solvents showed a marked effect on catalytic activity. Dielectric constant and miscibility with water are a measure of the polarity of the solvent. Gutmann's acceptor number (AN) determines the Lewis acidity of the solvent. A comparison of these physical parameters and catalytic activity data reveals that the polarity of solvent alone is not sufficient but a higher value of AN is also essential to get good activity and selectivity. Ethanol and iso-propanol have higher values of AN associated with high miscibility in water. Hence, they are the right choice of solvents to get high catalytic activity. Acetonitrile, in spite of being more polar and miscible with water, has lower value of AN and hence is not a good choice of solvent. Madon et al. [55], in hydrogenation of cyclohexene, found a dependence of turnover rates (at a given H_2 pressure) on the chemical entity of the solvent used. The concentration of dissolved H_2 is the crucial parameter that determined the reaction rate. The rate increased with the increasing liquid phase H_2 concentration, which depends on the nature of the solvent. Later, Madon and Iglesia [56] explained this solvent-induced non-ideal behavior effect in terms of transition state theory. They reported that the rates of catalytic reactions in the presence of solvents depend only when it influences the activated complexes involved in the kinetically significant steps in the catalytic cycle. Possibly, the same explanation holds good even in the present study.

Fig. 10 depicts the comparative catalytic activity of CeO_2–ZrO_2-supported Pt and Pd catalysts. The study on Pd catalysts was reported by us earlier [24]. While both these catalysts are equally active, they showed marked differences in the product selectivity.

Table 9
Catalytic activity of different supported Pt catalysts for hydrogenation of cinnamaldehyde.

Catalyst	Reaction conditions (amount of catalyst, temperature, H_2 pressure, reaction time)	CA conversion (%)	CAL selectivity (%)	Reference
Pt (14%)/zeolite-Y	0.4 g, 60 °C, 40 bar, 2 h	75	96	[44]
Pt(5%)/K-10 montmorillonite	0.02 g, 25 °C, 4 bar, 17 h	70	99	[45]
Pt(2%)/modified montmorillonite	0.3 g, 100 °C, 5 bar, 5 h	89	80	[46]
Pt(3%)/potassium titanate nanotube	0.05 g, 40 °C, 10 bar, 4 h	70	83	[47]
Pt(4%)-$FeCl_2$(0.2%)/charcoal	0.4 g, 60 °C, 40 bar, 2 h	75	87	[48]
Pt(2.2%)carbon nanofiber	0.1 g, 100 °C, 50 bar	90	68	[37]
Pt(5%)Fe(0.8%)Zn(0.4%)/mesoporous carbon	0.3 g, 100 °C, 16 bar, 12 h	96	86	[48]
Pt(3%)/multi-walled carbon nanotubes	0.4 g, 80 °C, 20 bar, 9 h	100	88	[42]
Pt(5%)/Cr–ZnO	0.3 g, 110 °C, 70 bar, 2 h	100	96	[20,49]
$PtSn_{0.8}/SiO_2$	0.2 g, 90 °C, 10 bar, 4 h	60	80	[50]
Pt(1%)/Al_2O_3	0.4 g, 60 °C, 40 bar, 2 h	90	64	[51]
Pt(5%)/CeO_2–ZrO_2	0.05 g, 25 °C, 20 bar, 8 h	95.8	93.4	This work

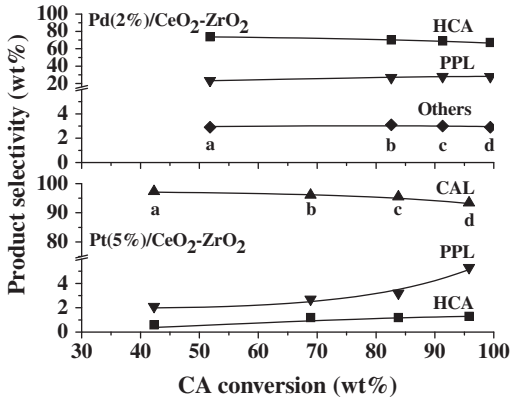

Fig. 10. Comparative catalytic activity of CeO_2–ZrO_2-supported Pd and Pt catalysts. *Reaction conditions*: Catalyst (0.05 g), cinnamaldehyde (CA, 4 g), solvent – ethanol (40 ml) for Pd and iso-propanol for Pt catalysts, alkali additive = 0.02 g of NaOH in 10 ml water, H_2 pressure = 20 bar, reaction temperature = 50 °C (for Pd) and 25 °C (for Pt). HCA = hydrocinnamaldehyde, PPL = 3-phenylpropanol, CAL = cinnamyl alcohol, others include acetals; *a* = 1 (for Pd) and 2 h (for Pt), *b* = 4 h, *c* = 6 h, and *d* = 8 h.

While the Pd catalyst is selective mainly for HCA at all conversion levels, Pt catalysts are selective for CAL. In other words, the nature of the metal influences the product selectivity. Delbecq and Sautet [11] reported that metal selectivities can be rationalized in terms of the different radial expansion of their d bands; the larger the band, the stronger the four-electron repulsive interactions with the C=C bond and the lower the probability of its adsorption. Indeed, the d band width increases in the series Pd < Pt < Ir, Os, which accounts well for the selectivities observed over Pd and Pt catalysts. The crystallite size (5–12 nm), preferential exposure of [1 1 1] plane, high dispersion (40.5%), high electron density, strong metal–support interactions, and facile low-temperature reducibility of Pt are the unique features that made Pt/CeO_2–ZrO_2 as a highly efficient and selective hydrogenation catalyst.

4. Conclusions

Intramolecular liquid phase hydrogenation of cinnamaldehyde was investigated over Pt (5 wt%) supported on CeO_2, ZrO_2, and CeO_2–ZrO_2 catalysts. Cinnamyl alcohol was obtained as the selective product. Structural and electronic factors, alkali promoters, and solvent influenced the catalytic properties. Acidity of the support (due to the presence of ZrO_2 component) and higher electron density at Pt (due to CeO_2 component) are responsible for the higher catalytic activity and selectivity of Pt supported on CeO_2–ZrO_2 composite material. These catalysts were highly active and selective even at 25 °C and found to be superior to most of the hitherto known supported Pt catalysts.

Acknowledgment

S.B. acknowledges the Council of Scientific and Industrial Research, New Delhi for the award of Senior Research Fellowship.

References

[1] P. Gallezot, D. Richard, Catal. Rev. Sci. Eng. 40 (1998) 81.
[2] P. Claus, Topic Catal. 5 (1998) 51.
[3] U.K. Singh, M.A. Vannice, Appl. Catal. A: Gen. 213 (2001) 1.
[4] P. Mäki-Arvela, J. Hájek, T. Salmi, D.Y. Murzin, Appl. Catal. A: Gen. 292 (2005) 1.
[5] K. Weissermel, H.J. Arpe, Industrial Organic Chemistry, Verlag Chemie, Weinheim, 1978.
[6] S. Mahmoud, A. Hammoudeh, S. Gharaibeh, J. Melsheimer, J. Mol. Catal. A: Chem. 178 (2002) 161.
[7] J. C Serrano-Ruiz, J. Luettich, A. Sepúlveda-Escribano, F. Rodríguez-Reinoso, J. Catal. 241 (2006) 45.
[8] P. Kluson, L. Cerveny, Appl. Catal. 128 (1995) 13.
[9] X.F. Chen, H.X. Li, Y.P. Xu, M.H. Wang, Chin. Chem. Lett. 13 (2002) 107.
[10] P. Claus, A. Brülckner, C. Mohr, H. Hofmeister, J. Am. Chem. Soc. 122 (2000) 11430.
[11] F. Delbecq, P. Sautet, J. Catal. 152 (1995) 217.
[12] T. Vergunst, F. Kapteijn, J.A. Moulijn, Catal. Today 66 (2001) 381.
[13] A. Dandekar, M.A. Vannice, J. Catal. 183 (1999) 344.
[14] B. Campo, M. Volpe, S. Ivanova, R. Touroude, J. Catal. 242 (2006) 162.
[15] K. Liberkova, R. Touroude, D.Y. Murzin, Chem. Eng. Sci. 57 (2002) 2519.
[16] S. Galvagne, A. Donato, G. Neri, R. Pietrepaele, C. Capannolli, J. Mol. Catal. 78 (1993) 227.
[17] S. Galvagne, C. Milone, A. Donato, G. Neri, R. Pietropaolo, Catal. Lett. 17 (1993) 55.
[18] J.Q. Wang, Y.Z. Wang, S.H. Zhe, M.H. Qiao, H.X. Li, K.N. Fan, Appl. Catal. A: Gen. 272 (2004) 29.
[19] D. Richard, J. Ockelford, A. Giroir-Fendler, P. Gallezot, Catal. Lett. 3 (1989) 53.
[20] E.V. Romos-Fernández, J. Ruiz-Martínez, J.C. Serrano-Ruiz, J. Silvestre-Albero, A. Sepúlveda-Escribano, F. Rodriguez-Reinoso, Appl. Catal. A: Gen. 402 (2011) 50.
[21] J. Teddy, A. Falqui, A. Corrias, D. Carta, P. Lecante, I. Gerber, P. Serp, J. Catal. 278 (2011) 59.
[22] M. Englisch, V.S. Ranade, J.A. Lercher, J. Mol. Catal. A: Chem. 121 (1997) 62.
[23] B. Coq, P.S. Kubhar, C. Moreau, P. Moreau, F. Figueras, J. Phys. Chem. 98 (1994) 10180.
[24] S. Bhogeswararao, D. Srinivas, Catal. Lett. 140 (2010) 55.
[25] M. Shen, J. Wang, J. Shang, Y. An, J. Wang, W. Wang, J. Phys. Chem. C 113 (2009) 1543.
[26] M. Shen, M. Yang, J. Wang, J. Wen, M. Zhao, W. Wang, J. Phys. Chem. C 113 (2009) 3212.
[27] M. Zhao, S. Chen, X. Zhang, M. Gong, Y. Chen, J. Rare Earths 27 (2009) 728.
[28] P. Bera, K.C. Patil, V. Jayaram, G.N. Subbanna, M.S. Hegde, J. Catal. 186 (2000) 293.
[29] H. Wang, Y. Chen, Q. Zhang, Q. Zhu, M. Gong, M. Zhao, J. Nat. Gas Chem. 18 (2009) 211.
[30] L. Vivier, D. Duprez, ChemSusChem 3 (2010) 654.
[31] M. Yashima, T. Hirose, S. Katano, Y. Suzuki, M. Kakihana, M. Yoshimura, Phys. Rev. B: Condens. Matter 51 (1995) 8018.
[32] S. Otsuka-Yao-Matsuo, T. Omata, N. Izu, H. Kishimoto, J. Solid State Chem. 138 (1998) 47.
[33] T. Omata, H. Kishimoto, S. Otsuka-Yao-Matsuo, N. Ohtori, N. Umesaki, J. Solid State Chem. 147 (1999) 573.
[34] G. Li, B. Zhao, Q. Wang, R. Zhou, Appl. Catal. B: Environ. 97 (2010) 41.
[35] A. Trovarelli, Catal. Rev. 38 (1996) 439.
[36] A. Martínez-Arias, M. Fernández-García, V. Ballesteros, L.N. Salamanca, J.C. Conesa, C. Otero, J. Soria, Langmuir 15 (1999) 4796.
[37] A. Jung, A. Jess, T. Schubert, W. Schütz, Appl. Catal. A: Gen. 362 (2009) 95.
[38] P. Hollins, Surf. Sci. Rep. 16 (1992) 51.
[39] A. Martínez-Arias, J.M. Coronado, R. Cataluña, J.C. Conesa, J. Soria, J. Phys. Chem. B 102 (1998) 4357.
[40] J.R. Croy, S. Mostafa, L. Hickman, H. Heinrich, B. Roldan Cuenya, Appl. Catal. A: Gen. 350 (2008) 207.
[41] M. Dömök, A. Oszkó, K. Baán, I. Sarusi, A. Erdöhelyi, Appl. Catal. A: Gen. 383 (2010) 33.
[42] Z.-T. Liu, C.-X. Wang, Z.-W. Liu, J. Lu, Appl. Catal. A: Gen. 344 (2008) 114.
[43] E. Bekyarova, P. Fornasiero, J. Kašpar, M. Graziani, Catal. Today 45 (1998) 79.
[44] P. Gallezot, A. Giroir-Fendler, D. Richard, Catal. Lett. 5 (1990) 169.
[45] G. Szöllösi, B. Török, L. Baranyi, M. Bartók, J. Catal. 179 (1998) 619.
[46] D. Manikandan, D. Divakar, T. Sivakumar, Catal. Commun. 8 (2007) 1781.
[47] C.-Y. Hsu, T.-C. Chiu, M.-H. Shih, W.-J. Tsai, W.-Y. Chen, C.-H. Lin, J. Phys. Chem. C 114 (2010) 4502.
[48] N. Mahata, F. Conçalves, M. Fernando, R. Pereira, J.L. Figueiredo, Appl.Catal. A: Gen. 339 (2008) 159.
[49] E.V. Ramos-Fernández, A.F.P. Ferreira, A. Sepúlveda-Escribano, F. Kapteijn, F. Rodríguez-Reinoso, J. Catal. 258 (2008) 52.
[50] A.J. Plomp, D.M.P. van Asten, A.M.J. van der Eerden, P. Mäki-Arvela, D.Y. Murzin, K.P. de Jong, J.H. Bitter, J. Catal. 263 (2009) 145.
[51] A. Giroir-Fendler, D. Richard, P. Gallezot, Catal. Lett. 5 (1990) 175.
[52] D. Loffreda, F. Delbecq, F. Vigné, P. Sautet, Angew. Chem. Ind. Ed. 44 (2005) 5279.
[53] D. Loffreda, F. Delbecq, F. Vigné, P. Sautet, J. Am. Chem. Soc. 128 (2006) 1316.
[54] J.C. Serrano-Ruiz, A. López-Cudero, J. Solla-Gullón, A. Sepúlveda-Escribano, A. Aldaz, F. Rodríguez-Reinoso, J. Catal. 253 (2008) 159.
[55] R.J. Madon, J.P. O-Connell, M. Boudart, AIChE J. 24 (1978) 904.
[56] R.J. Madon, E. Iglesia, J. Mol. Catal. A: Chem. 163 (2000) 189.